Supporting Information

Lafont et al. 10.1073/pnas.0902599107

SI Materials and Methods

Animals. Under anesthesia, respiration was regulated using a small animal ventilator (SAR-830P, CWE, Inc.), and depth of anesthesia was assessed by monitoring pinch withdrawal and whisker movement. A custom-made holder was used to immobilize the skull, which was fixed with cyanoacrylate glue onto a glass slide. Body temperature was monitored by a rectal probe and maintained at 37 °C by a heating blanket (Homeothermic Blanket Control Unit; Harvard Apparatus), and heart rate was continuously monitored (Powerlab; AD Instruments). For superfusion, the physiological solution was (in mM) 125 NaCl, 2.5 KCl, 1.25 NaH_2PO_4, 26 $NaHCO_3$, 12 glucose, 2 $CaCl_2$, and 1 $MgCl_2$ (pH 7.4) when bubbled with 95% O_2/5% CO_2. For oxygen tension monitoring, the superfusion solution was 0.9% NaCl and 5 mM Hepes (pH 7.4).

All animal studies complied with the animal welfare guidelines of the European Community and/or UK Home Office guidelines, as appropriate. They were approved by the Languedoc Roussillon Institutional Animal Care and Use Committee (CE-LR-0818).

Long Working Distance Imaging with Cellular Resolution and Analysis. Long working distance objectives: M Plan Apo ×20, 0.43 NA, 2.8 cm WD; x20, 0.60 NA, 1.3 cm WD; all from Mitutoyo. Fluorescence excitation was delivered by a Lambda LS xenon arc lamp (300W; Sutter Instruments) fitted with a fast-rotating filter wheel (27 ms lag) and linked to the stereomicroscope with an optical fiber. Fluorescence emission was captured by an EM-CCD camera 512 × 512 C9100 (Hamamatsu) and acquired with MetaMorph software (Molecular Devices). New software tools were developed to correct images (registration) for movement due to respiration or blood pressure and for blood flow analysis. The registration tool is based on a subpixel translation obtained from a minimal image difference search. Blood flow was obtained from a statistical analysis of time-space diagrams of the intensities along defined capillary paths. All of the software tools were implemented in the ImageJ environment, with registration and velocity calculations made with two different plugins. The software tools can be freely downloaded from http://ipam.igf.cnrs.fr/en/index.php?page=how-cmsms-works.

Blood Flow Measurements, Oxygen Tension Monitoring, and Dye Injections. Oxygen electrodes with a tip diameter of 2–5 μm were calibrated at 37 °C before experiments, first in saline with 21% oxygen (air saturated) and then in 0% oxygen (bubbled with nitrogen). The data were acquired at 10 Hz (Powerlab; AD Instruments). In some experiments, $P_{tiss,O2}$ was measured in acute pituitary slices, which were made as previously reported (1). Pituitary slices were continuously perfused with Ringer solution buffered with 20 mM hepes at pH 7.4 (2, 3).

Fluorescent dextrans were introduced by iontophoresis (Microiontophoresis Dual Current Generator 260; World Precision Instruments) from a glass micropipette introduced under visual guidance, avoiding blood vessels. Iontophoretic rather than hydrostatic injections were used to minimize pressure/flow artifacts, and repeated injections showed that similar observations could be repeatedly obtained at different local sites in the field. Images were analyzed using the ImageJ plugins described previously.

To assess $P_{tiss,O2}$ differences before and after i.v. GHRH injection, a two-tailed variance ratio test (F test) was used. Blood flow changes were assessed using a two-tailed variance ratio test followed by a Mann–Whitney U test to assess any differences directly attributable to treatment application (Fig. 3C). In all cases, treatment effects were considered significant at $P < 0.05$ (4).

Calcium and Electrophysiological Recordings. To monitor cytosolic calcium, cells were loaded with the fluorescent calcium dye fura-2/AM after bolus injection via a micropipette (pressure 0.2 bar during 2 min) controlled with a MP-285 micromanipulator (Sutter Instruments). A wheel splitter (Lambda 10-B; Sutter Instruments) in the xenon arc lamp enabled us to change the excitation wavelength in 27 ms without any vibrations of the stereomicroscope. Correlation coefficients were calculated on smoothed and detrended calcium time series using a lagged cross-correlation analysis of Fourier transforms (Fig. S2C). Positive correlation values were taken from the origin and plotted as a function of distance to create a correlation map. All analysis was performed using GraphPad Prism v5 (GraphPad Software Inc.) and Matlab (Mathworks Inc.). Electrical activity (5) was monitored with extracellular microelectrodes filled with 150 mM NaCl, 12.5 mM KCl, 0.5 mM Lucifer yellow (lithium salt) and Hepes (pH 7.4) connected to an AxoClamp 2B amplifier and the software Axoclamp (Axon Instruments).

Multiphoton and Confocal Imaging of GH-EGFP Pituitaries. For multiphoton and confocal imaging, pituitaries were collected on ice and fixed overnight in 4% paraformaldehyde. Multiphoton imaging was performed with a Zeiss LSM 510 NLO confocal system (25× oil, 0.8 NA). Multiphoton excitation was achieved with a mode-locked Ti:Sapphire Laser Chameleon (Coherent Inc.) tuned at 840 nm (pulse duration <140 fs) (1). Emitted fluorescence was recorded from 500 to 550 nm for GFP signals and from 610 to 700 nm (on META detector) for rhodamine signals. Confocal imaging was performed with a Zeiss LSM 510 META confocal system (10×, 0.3 NA). In multitrack mode, GFP signals were collected between 505 and 530 nm with 488 nm excitation, and rhodamine signals between 560 and 615 nm with 543 nm excitation.

1. Bonnefont X, et al. (2005) Revealing the large-scale network organization of growth hormone-secreting cells. *Proc Natl Acad Sci USA* 102:16880–16885.
2. Jung SK, Aspinwall CA, Kennedy RT (1999) Detection of multiple patterns of oscillatory oxygen consumption in single mouse islets of Langerhans. *Biochem Biophys Res Commun* 259:331–335.
3. Ortsäter H, Liss P, Lund PE, Akerman KE, Bergsten P (2000) Oscillations in oxygen tension and insulin release of individual pancreatic ob/ob mouse islets. *Diabetologia* 43:1313–1318.
4. Zar JH (1999) *Biostatistical Analysis* (Prentice Hall, Englewood Cliffs, NJ).
5. Baccam N, et al. (2007) Dual-level afferent control of growth hormone-releasing hormone (GHRH) neurons in GHRH-green fluorescent protein transgenic mice. *J Neurosci* 27:1631–1641.

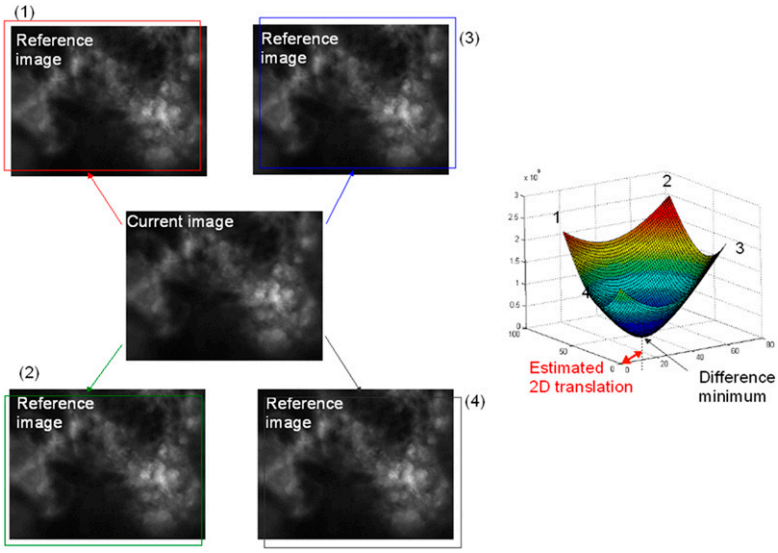

Fig. S1. To correct the movies for animal movement, we used a registration method based on minimal distance evaluation. The average distance from any image of the movie to a reference image (usually the first one) was calculated for eight different trial translations. A parabolic interpolation of these distance values lead to a minimum, and the corresponding image-specific translation—usually fractional in terms of pixels—was then applied to the whole image stack. See also Movie S1.

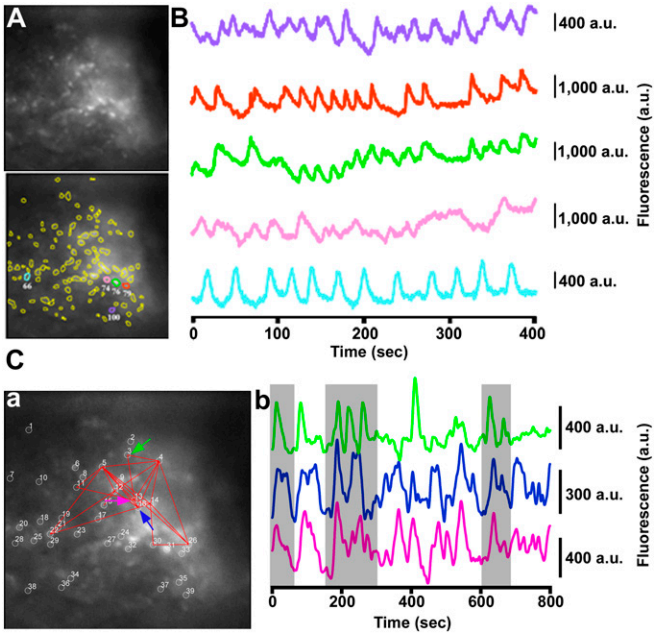

Fig. S2. In vivo calcium imaging of pituitary cells. (*A Top*) Overview of a field of the ventral pituitary following fura-2/AM loading with the multibolus cell loading protocol. (*Bottom*) Same pituitary field with regions of interest (ROIs) corresponding to fura-2-labeled cells. (*B*) Time-lapse recording of cytosolic calcium activities in representative cells delimited with colored ROIs. (*C a* and *b*) Cross-correlogram analysis between calcium recordings among spontaneously active cells. Red lines link cell pairs with $R > 0.5$. Colored arrows indicate cells from which calcium recordings are illustrated in *b*. Vertical gray bands point out some episodes of highly correlated calcium activities between these three cells. See also Movie S2.

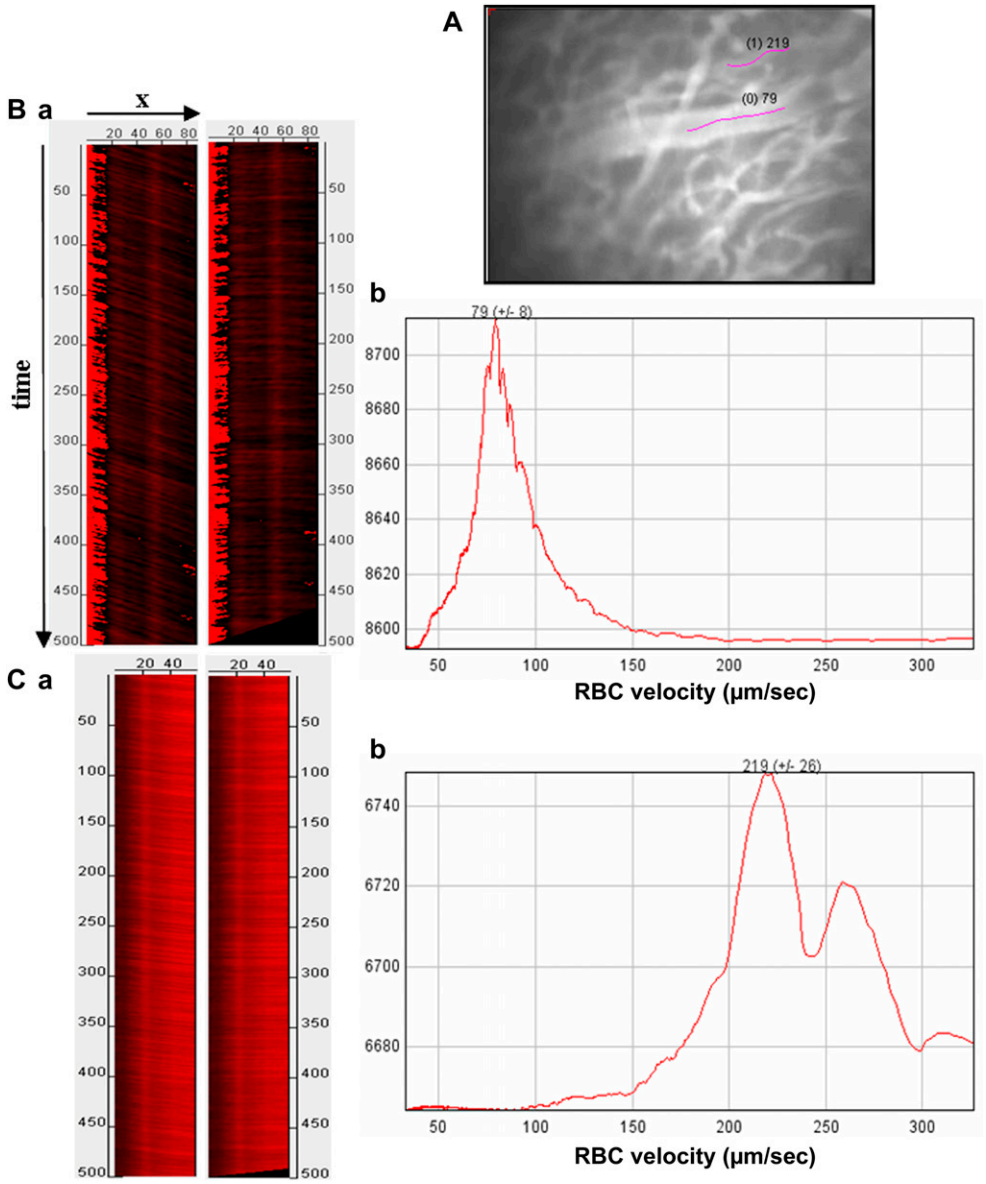

Fig. S3. (*A*) Paths were semiautomatically defined along the capillaries of interest. Vessels 0 and 1 correspond to RBC velocities described in *B* and *C*, respectively. (*B* and *C*) (*a*) For each vessel branch, an x-t diagram was plotted (*Left*); each line corresponds to the intensity signal along this path, for a given time frame. Homothetic transformation of the x-t diagram was performed along the vertical direction to align the oblique stripes horizontally (*Right*). Each homothetic transform was associated with an angle of rectification, which was equivalent to a trial velocity. A contrast index helped measure the degree of horizontal alignment. (*b*) This index was then plotted against the velocities, and the maximum indicated the velocity of the capillary. Top values reported as means ± SD.

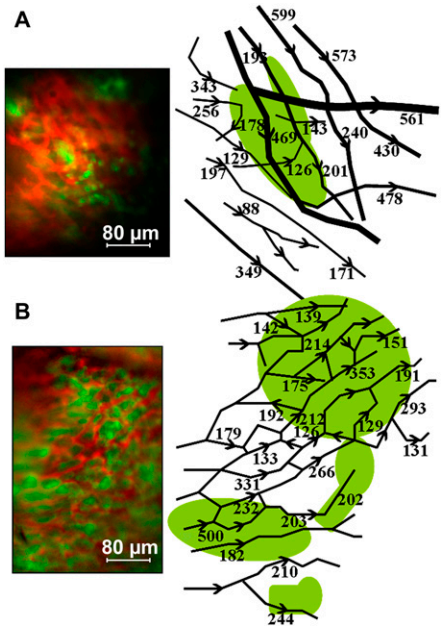

Fig. S4. Regional RBC velocities in GH-eGFP mice. (*A* and *B*) Maps of microcirculation in mediorostral and laterocaudal regions of a GH-GFP pituitary, respectively. The schematics (*Right*) indicate RBC velocities and blood flow directions (arrows). The green zones represent GH cell mass in these fields.

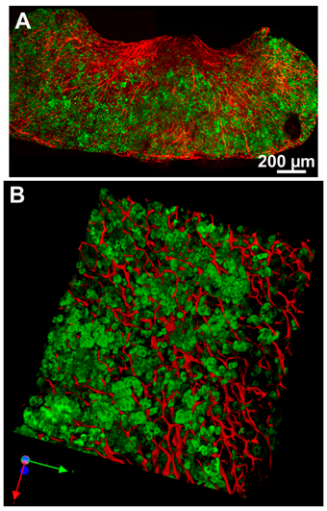

Fig. S5. Vascular architecture of male GH-GFP mice. (*A*) Pituitary-scale 3D distribution of blood vessels (filled with gelatin-rhodamine) in a GH-eGFP pituitary imaged with confocal microscopy. (*B*) High-magnification 3D imaging of both blood vessels and the GH cell network in a GH-GFP pituitary imaged with two-photon excitation microscopy. 3D reconstruction of a 96-μm-thick image stack (x size, 400 μm; y size, 360 μm).

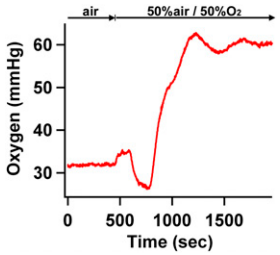

Fig. S6. Resting $P_{tiss,O2}$ levels upon changes in breathing O_2 concentration. Resting pituitary $P_{tiss,O2}$ levels were monitored with Clark-type oxygen microsensors in anesthetized GH-eGFP mice. Note that the changes in inspired O_2 concentration led to a stepwise change in resting $P_{tiss,O2}$ levels.

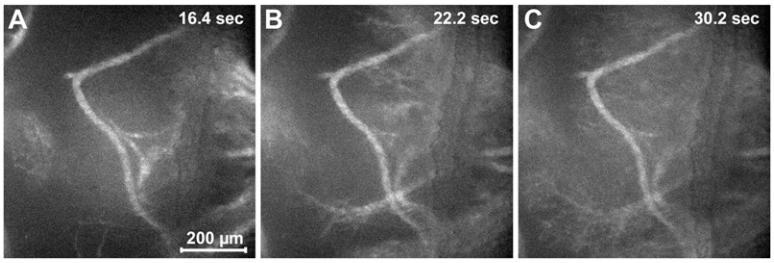

Fig. S7. In vivo imaging of incoming molecules thought the microvasculature at low magnification. Time-lapse imaging of 4 kDa rhodamine-dextran in pituitary vessels, with the palate bone polished (Movie S4). Values indicate the time delay after dye injection. Right–left direction shows the rostrocaudal orientation of the gland.

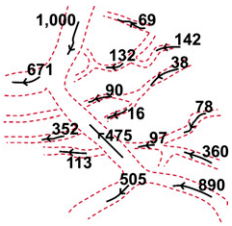

Fig. S8. RBC velocities in the microcirculation of the GH-eGFP mouse illustrated in Fig. 5*A*. Schematics of vessel locations (red dashed lines), RBC velocities in vessel branches, and blood flow directions (arrows). These were estimated after i.v. injection of 500 kDa fluorescein dextran.

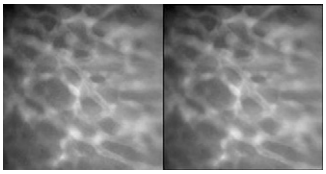

Movie S1. Movie of a pituitary field registered in vivo before (*Left*) and after (*Right*) movement registration, respectively (Fig. S1).

Movie S1

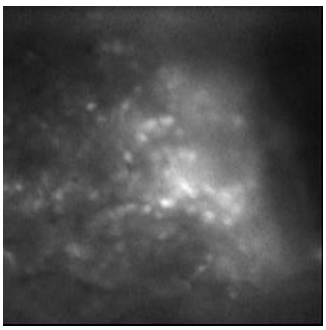

Movie S2. In vivo calcium spiking in pituitary cells (Fig. S2).

Movie S2

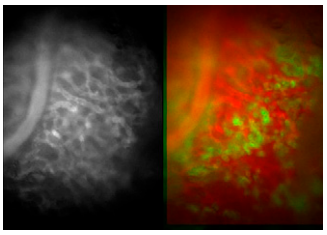

Movie S3. In vivo imaging of rhodamine dextran-labeled vasculature (*Left*) and corresponding RBC velocities in vessel branches (red) in a GH-eGFP (green) pituitary (Fig. 2*A*).

Movie S3

Movie S4. Low-magnification pituitary distribution of 4-kDa rhodamine-labeled dextran, which was injected i.v. (Fig. S7).

Movie S4

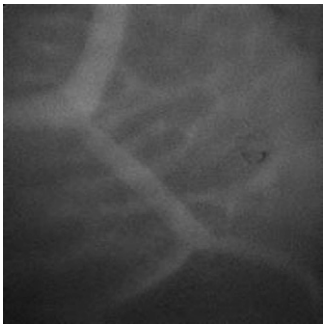

Movie S5. High-magnification pituitary distribution of 4-kDa rhodamine-labeled dextran, which was injected i.v. (Fig. 5*A*).

Movie S5

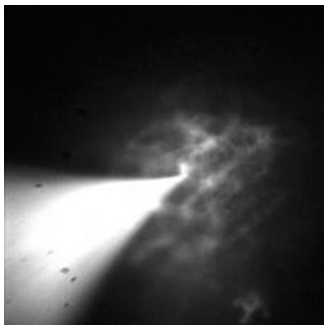

Movie S6. Pituitary distribution of 4-kDa rhodamine-labeled dextran, which was iontophoretically injected into the parenchyma (Fig. 5*B*). The movie rate was increased 3-fold. Inspection of the movie clearly shows that the initial introduction of fluorescent markers is confined and distant from some uptake sites, that the smaller-sized dextrans move evenly toward, and are rapidly cleared by, the local microvasculature.

Movie S6

Movie S7. Pituitary distribution of 20-kDa FITC-labeled dextran, which was iontophoretically injected into the parenchyma (Fig. 5*D*).

Movie S7